AFCRL-62-1136
DECEMBER 1962

63-35

Research Report

Upper Atmosphere Density Obtained from Falling Sphere Drag Measurements

G. A. FAUCHER
R. W. PROCUNIER
F. S. SHERMAN

SPACE PHYSICS LABORATORY PROJECT 6690

AIR FORCE CAMBRIDGE RESEARCH LABORATORIES, OFFICE OF AEROSPACE RESEARCH, UNITED STATES AIR FORCE, L.G. HANSCOM FIELD, MASS.

Requests for additional copies by Agencies of the Department of Defense, their contractors, and other government agencies should be directed to the:

Armed Services Technical Information Agency
Arlington Hall Station
Arlington 12, Virginia

Department of Defense contractors must be established for ASTIA services, or have their 'need-to-know' certified by the cognizant military agency of their project or contract.

All other persons and organizations should apply to the:

U. S. DEPARTMENT OF COMMERCE
OFFICE OF TECHNICAL SERVICES,
WASHINGTON 25, D. C.

AFCRL-62-1136
DECEMBER 1962

Research Report

Upper Atmosphere Density Obtained from Falling Sphere Drag Measurements

G. A. FAUCHER
R. W. PROCUNIER
F. S. SHERMAN*

*University of California, Berkeley, California

SPACE PHYSICS LABORATORY PROJECT 6690

AIR FORCE CAMBRIDGE RESEARCH LABORATORIES, OFFICE OF AEROSPACE RESEARCH, UNITED STATES AIR FORCE, L.G. HANSCOM FIELD, MASS.

Abstract

A density profile vs altitude from 95 to 130 km, obtained from drag measurements made directly from within a falling sphere, are presented. The main sensors are linear accelerometers aligned to measure X, Y, Z components of acceleration of the sphere from which total drag is obtained. The method consists of ejecting an inflatable sphere somewhere between 80 and 100 km on the ascent of an Aerobee 150 rocket flight. From ejection, the sphere continues to approximately 250 km altitude on a trajectory which is, except for drag, a free-fall trajectory.

The prediction of sphere drag coefficients with their estimated probable errors are given in the altitude range from 90 to 160 km and was made by Prof. Frederick S. Sherman of the University of California. The telemetry record showing the drag forces used in calculating the density profile in the altitude range 95 to 130 km is shown in Figure 10. The sources of error in the calculated density are analyzed and tabulated. The calculated density in kilograms per cubic meters vs altitude in kilometers is compared with the ARDC Model Atmospheres of 1956, 1959, and 1961.

Contents

Illustrations

Upper-Atmosphere Density Obtained From Falling Sphere Drag Measurements

1. INTRODUCTION

This paper gives the density profile vs altitude from 95 to 130 km obtained from drag measurements made directly from within a falling sphere. The method consists of ejecting an inflatable sphere, 2.74 m in diameter, somewhere between 80 and 100 km during the ascent of an Aerobee 150 rocket flight. At the center of the sphere, supported by an inflated cylincrical strut (see Figure 1), are the measuring instruments and the necessary electronics to telemeter the information continuously throughout the flight. The main sensors are linear accelerometers aligned to measure the X, Y, Z components of acceleration of the sphere from which total drag is obtained. From ejection altitude, the sphere continues to an altitude of approximately 250 km on a trajectory which is, except for drag, a free-fall trajectory. Measurements obtained by this method are supplemented by tracking systems for velocity and position.

The drag acceleration a_D is related to the drag force D and, in turn, the drag force is a function of the air density by the classical equation

$$D = m a_D = \frac{\rho C_D A V^2}{2}, \qquad (1)$$

(Authors' manuscript approved for publication, 27 November 1962)

Figure 1. Inflated Sphere with Instrument Package Suspended at Center

in which m is the mass accelerated by the drag force, A is the sphere cross-sectional area, V is the sphere velocity, C_D is the coefficient of drag, and ρ is the atmospheric density. In this experiment, m and A are known, a_D and V are measured, and C_D or ρ can therefore be calculated if one is assumed or determined independently. The authors believe at this time that the drag coefficients available are more accurate than the present estimates of atmospheric density in the altitude range investigated.

This rocket firing is the second of a series designed, constructed, and instrumented by project personnel of the Geophysics Research Directorate, Air Force Cambridge Research Laboratories.

For economical reasons the first flight was a prototype and was successfully flown in a Nike Cajun sounding rocket (AA6.170) on 23 February 1961. The flight information and experimental results of the first flight of the falling sphere system for measuring upper-air density was reported by Faucher, Procunier, and Stark.[1]

Previous uses of the falling sphere were developed by the University of Michigan. The first approach[2] was to eject an inflatable sphere, 4 ft in diameter, from an Aerobee rocket and measure the trajectory by means of the Dovap tracking system[4] and a Dovap transponder in the sphere. This method is limited by the accuracy of tracking, which is within a few feet.

The second approach was to measure acceleration directly from within the sphere, using a transit-time accelerometer in an aluminum sphere measuring 7 inches in diameter and weighing 11 pounds. The accelerometer compares the position of the drag-accelerated sphere with the position of a free-falling mass within the sphere. This is in contrast to measuring the total acceleration by a ground tracking device and subtracting the acceleration of gravity to find the small difference, namely, the drag acceleration. This second approach results in improved sensitivity, even though a small (7-inch) metal sphere is used in place of the 4-ft inflatable sphere which has a more favorable mass-to-area ratio.[3,5,6]

To utilize this technique at significantly higher altitudes, it was necessary to increase accelerometer sensitivity and/or decrease the mass-to-area ratio of the sphere as well as to propel it to a higher velocity. Single-axis accelerometers were used because they can provide more information. The transit-time accelerometer, which gave average acceleration over an elapsed time, may give the correct result but only if spurious accelerations are negligible. As may be seen in Figure 10, page 15, this is not necessary in the case of a continuous-reading instrument.

2. INSTRUMENTATION

The test vehicle for this experiment was an Aerobee 150 sounding rocket, AB3.344. It carried a payload consisting of a folded instrumented sphere, radar beacons, telemetry transmitter, a de-spin, and range safety extensions. The sphere was constructed of 1-mil Mylar laminated with 2.25 oz/yd^2 dacron scrim. When released, it expanded to a diameter of 2.74 m. The inflated sphere had an internal pressure of 3 mmHg with 100 cc of methanol, and a pressure of 100 mmHg was obtained in each half of the strut with 24 cc of isopentane. Inflation time of the sphere and strut was approximately 8 sec. Figure 1 shows the inflated sphere with its instrument package suspended at center.

The folded sphere was ejected from the rocket by a 'slingshot' arrangement, utilizing four strips of neoprene that were stretched across the diameter of the nose cone (see Figure 2). The sphere was ejected with a force of approximately 300 lb, giving an ejection velocity of approximately 9 ft/sec.

Figure 3 shows the instrument package. It consists of an aluminum cylinder with caps and collapsible turnstile antennae, and is 6 inches in diameter, 20 inches long, and 15 lb in weight. Figure 4 is a block diagram of the instrumentation, which includes three separate subcarrier channels of orthogonal acceleration measurements and three time-shared accelerometers plus two internal temperature measurements on a fourth subcarrier frequency. The main sensors are six Donner Scientific Company Model 4310 linear accelerometers. They operate as subminiature servo

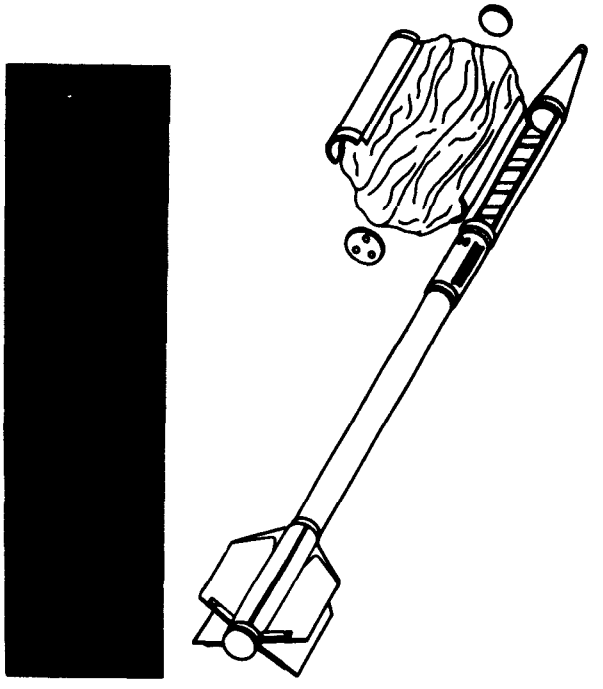

Figure 2. Inflatable Sphere Container and Nose Cone

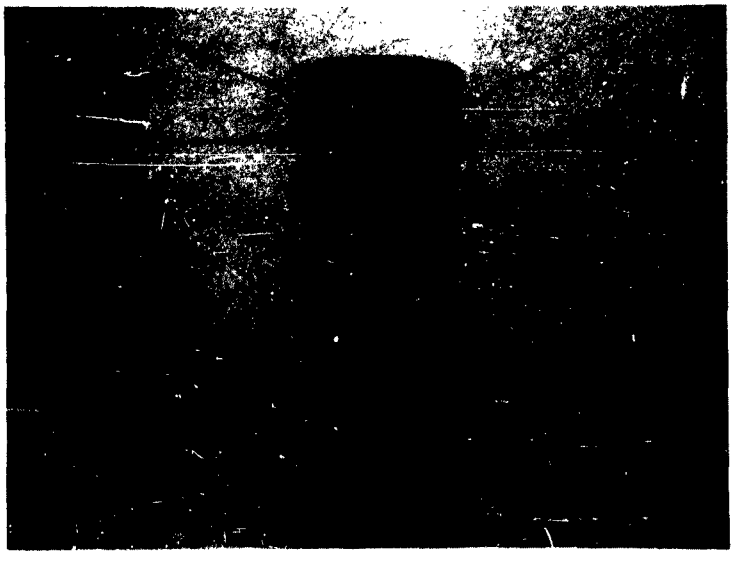

Figure 3. Sphere's Instrument Package

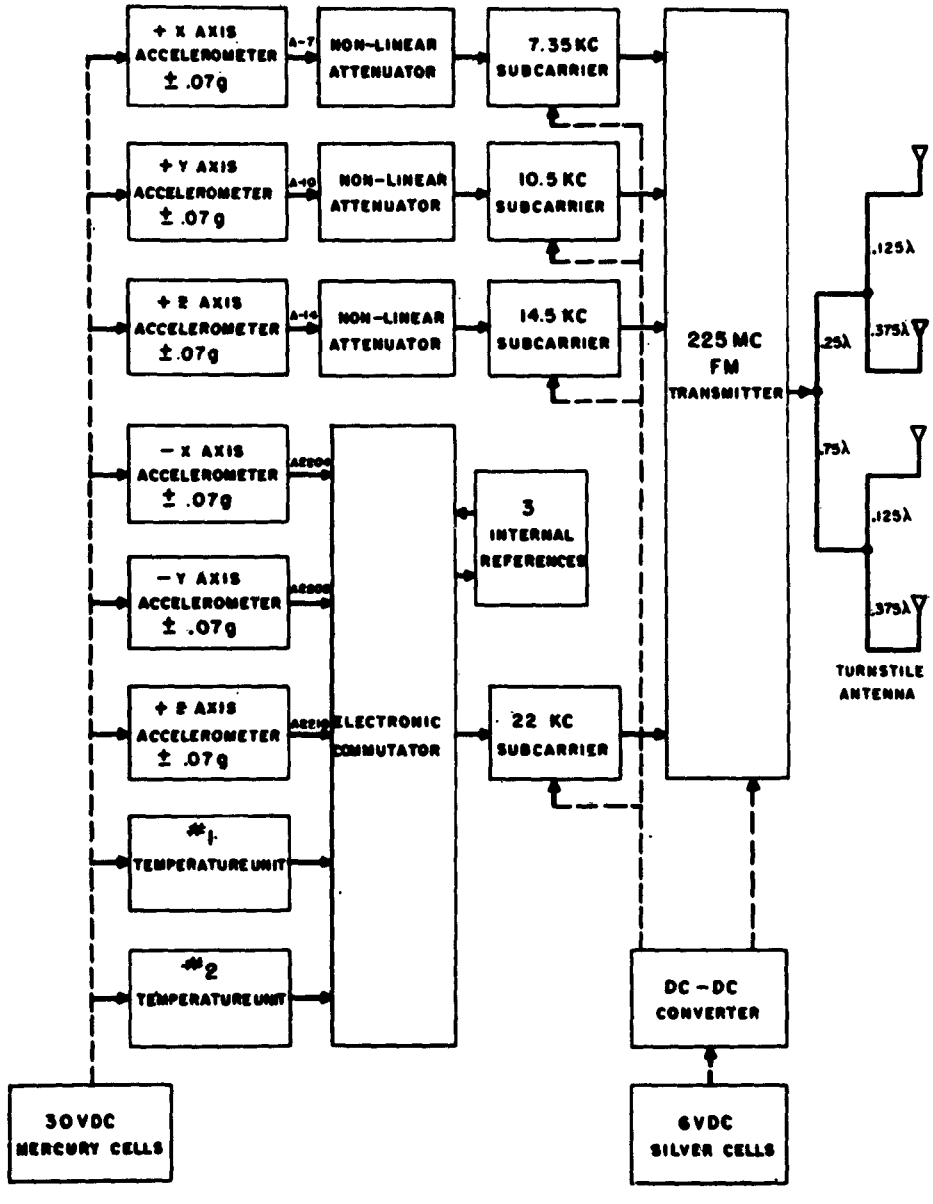

Figure 4. Simplified Block Diagram of Instrument Package

systems responsive to input linear acceleration along their sensitive axes. Basically the accelerometer is comprised of a seismic system and associated position-error detector, a restoring mechanism, and a servo error-signal amplifier.

The rocket and sphere were tracked by use of two AN/FPS-16 and one AN/MPS-19 radars; and one AN/FPS-16 was also used in skin tracking the sphere after ejection. In addition nine contravies phototheodolites were used to track the vehicle and the sphere, while two MATTS (Multiple Airborne Target Trajectory System) stations tracked the telemetry signals from the sphere.

The accelerometers are calibrated by tipping the units into the earth's gravity field. The local vertical determines the maximum value of one 'G' or 9.8035 m/sec^2, depending upon local value. As the sensitive axis is lowered from this peak, decreasing values of acceleration appear as inputs to the unit in the relationship $A = G \sin\theta$, where A is the acceleration input to the accelerometer, G is the local value of gravity, and θ is 90° minus the angle the sensitive axis makes with the local vertical. As the angle with the vertical becomes larger and approaches 90°, θ becomes 0° and A becomes 0. A 90° dip is all that is required to calibrate from zero to one G. For this experiment one need only calibrate from 0.0001 to 0.1 G, which represents an angle of about 6°.

The small angle is determined very accurately with the help of a double sine bar in an area where the noise level is below 10^{-5} G. The linearity and repeatability of the accelerometer were measured by attaching the accelerometer to the face plate of a Leitz dividing head and computing the values of acceleration from the sine of the angle. (See Figures 5 and 6.)

3. PREDICTION OF DRAG COEFFICIENT

The sphere, in the altitude range from 160 km to 90 km, falls through all the recognized regimes of rarefied gas flow, being in free-molecular flow at the top and in laminar boundary-layer flow at the bottom of this range. In general C_D will depend upon the Mach number (or molecular speed ratio), Reynolds number, ratio of sphere temperature to ambient temperature, atmospheric composition, and the 'reflection coefficients' that characterize the degree to which molecules leave the sphere surface in thermodynamic equilibrium with it. Fortunately, not all these factors are important in every range of altitude.

To make specific estimates of C_D *vs* altitude, one must first calculate M, Re, Kn, and T_w/T_o *vs* H, using best prior estimates of atmospheric structure at the time of flight. For this purpose, the ARDC Model Atmosphere, 1959 was used. Viscosities and mean free-paths were estimated from a simple Sutherland formula (see Table 1, page 11) that ignores changes in atmospheric composition.

Figure 5. Calibrating Accelerometers with Double Sine Bar

Figure 6. Obtaining Linearity of the Accelerometers with a Leitz Dividing Head

According to these estimates the sphere was in free-molecular flow at 140 km and above. At altitudes where drag data could be sensed with reasonable accuracy, 135 to 95 km, the sphere was in the transition regime and the boundary-layer regime.

3.1 Near-Continuum Flow

For altitudes between 110 and 90 km the sphere encountered conditions of Mach number, Reynolds number, and T_w/T_o very nearly identical to those investigated by Aroesty[7] in the University of California low-density wind tunnel. His results are substantially corroborated by the experiments of Ashkenas[8] and Sreekanth.[9] While the absolute temperature level of the sphere flight was higher than that of the wind-tunnel tests, no appreciable deviations from thermally perfect gas behavior should have appeared in either case. The dependence of viscosity upon temperature, which influences the conversion between Re_∞ and Re_2, differs appreciably between flight and wind-tunnel conditions; and it has been assumed that Re_2, rather than Re_∞, is the important Reynolds number for this problem. In Figure 7 the predicted curves of C_D *vs* Re_2 are essentially reproductions of Aroesty's data for $Re_2 > 22$ at $M = 6$, $Re_2 > 7$ at $M = 4$, and $Re_2 > 6$ at $M = 2$. The curve for $M = 3$ is interpolated.

3.2 Free-Molecular Flow

Above 140 km the Knudsen number exceeded five, and free-molecular flow was assumed. Although no drag data were obtained at these altitudes, a few observations will be made about the prediction of C_D for free-molecular conditions, since they may be useful in planning future experiments of this type and they are used here in an interpolation formula for transition flow.

The basic free-molecular drag theory for a pure gas is given by Schaaf and Chambré.[10] Upon the assumption that each component of a mixed gas acts independently, the drag coefficient for a sphere is given by

$$C_D = \sum_i n_i m_i C_D(s_i, s_{w_i}) / \sum_i n_i m_i, \tag{2}$$

where n_i and m_i are the number density and particle mass of the i^{th} species. For each species the authors use Equation (8-6) of Schaaf and Chambré.[10]

$$C_{D_{diff}} = \frac{e^{-s_i^2/2}}{\sqrt{\pi}} \left(\frac{1+2s_i^2}{s_i^3} \right) + \frac{4s_i^4+4s_i^2-1}{2s_i^4} \operatorname{erf}(s_i) + \frac{2\sqrt{\pi}}{s_{w_i}} \tag{3}$$

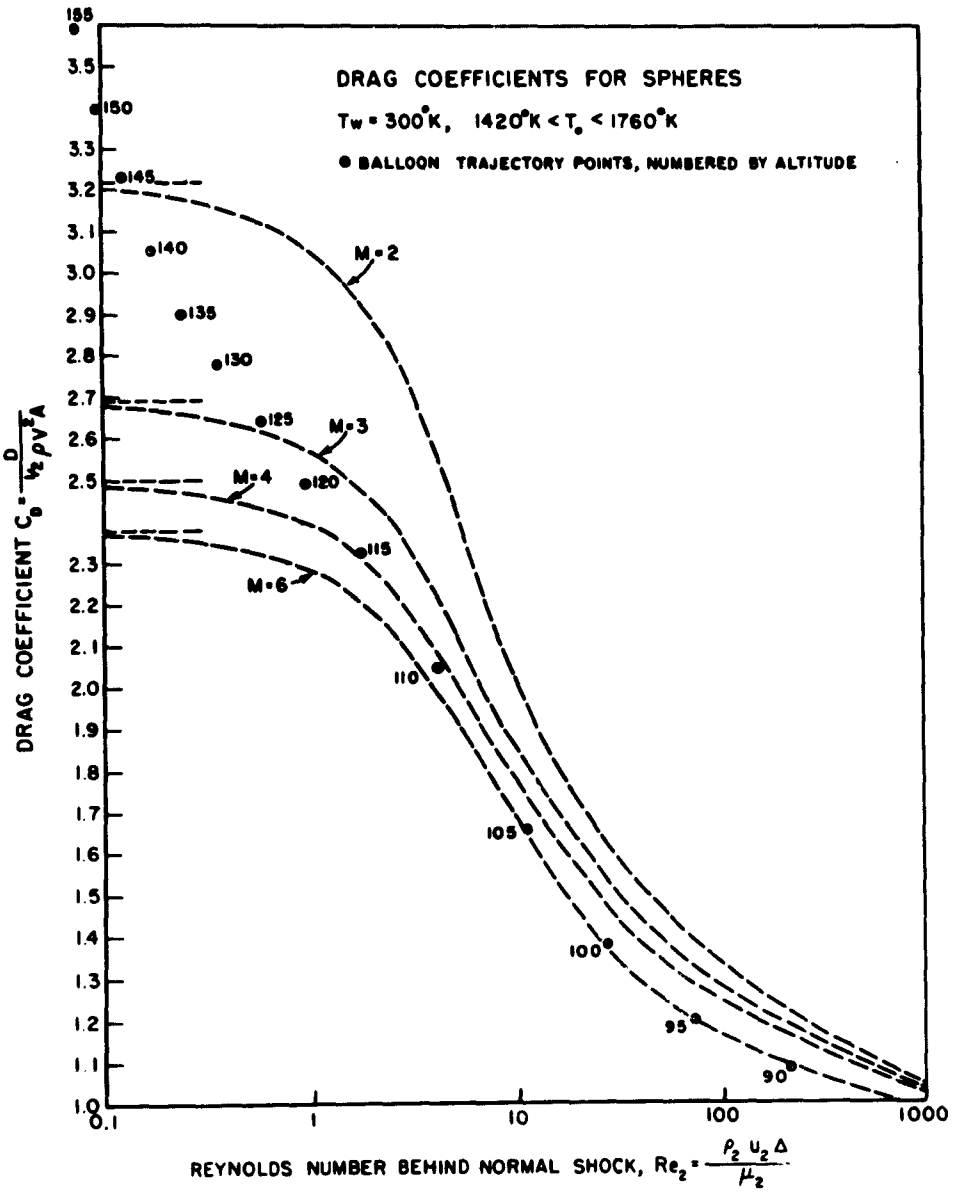

Figure 7. Predicted Curves of C_D vs Re_2

where

$$s_i = V\sqrt{\frac{m_i}{2kT}} \ , \ s_{w_i} = V\sqrt{\frac{m_i}{2kT_w}} \ .$$

V is the sphere velocity, relative to the atmosphere; T_w is the sphere surface temperature, assumed to be uniform; and T is the kinetic temperature of the atmosphere, which is assumed to have a local Maxwellian distribution of molecular velocities. T is assumed to be the same for all molecular species, and all species are supposed to be electrically neutral.

The principal questionable assumption underlying these equations is that each species of particle, after striking the sphere, is re-emitted in a Maxwellian effusion at the temperature and macroscopic velocity of the sphere, but with unchanged molecular or atomic identity. The accuracy of this assumption is expected to be quite good for surface materials such as the fabric used on the present sphere, which is microscopically rough but chemically noncatalytic for oxygen recombination.

An important implication of Eq. (3) is that C_D becomes quite insensitive to atmospheric temperature and composition if the flight speed is such that all the speed ratios s_i are ≥ 3. On the other hand, the nature of the reflection or re-emission of molecules at the sphere surface can be reasonably well predicted from laboratory experiments if the average kinetic energy of the atmospheric particles relative to the sphere is less than about 1 ev. For the altitude range from 100 to 200 km, a sphere speed of about 3000 m/sec would be ideal in both respects. As examples of the errors in C_D that result from uncertainties about temperature and composition, three values of C_D for h = 160 km have been contrasted. The value $C_D = 3.81$ given in Table 1 comes from using the ARDC 1959 Model Atmosphere and treating the atmospheric mixture as a pure gas having a mean molecular weight. Using the NASA 1962 (Harris and Priester[11]) atmospheric model, and again treating the mixture as an equivalent pure gas, gives $C_D = 3.33$. Finally, use of the NASA 1962 model and treating N_2, O_2, and O separately will give $C_D = 3.33$. If these same calculations are repeated, with the sphere speed doubled, the corresponding results are 2.54, 2.43, and 2.46, reducing the total spread of values from 14 percent to 4.5 percent.

3.3 Transition Flow

Between 110 and 140 km the sphere was in transition flow, for which very little directly pertinent theory or experimental data exist. The nearly-free-molecular flow theories do not seem to be successful as they stand,* and the authors resort

*See Maslach and Schaaf[12] for a critical review.

TABLE 1.

Z km	ρ kg/m^3	T ^oK	μ^* mks	V m/s	S	S_w	$C_{D_{F.M.}}$	Re_∞	$M^\dagger$	Re_2	$T_o{}^\dagger$ ^oK	T_w/T_o (Pred.	C_D Value)	Note
90	2.85×10^{-6}	166	1.12-5	1652				1148.	6.39	218.	1520	.197	1.08	A
95	9.91×10^{-7}	180	1.22-5	1622				363.	6.01	75.6	1480	.202	1.19	A
100	3.73-7	199	1.32-5	1591				123.	5.61	28.0	1450	.207	1.38	A
105	1.54-7	218	1.43-5	1561				46.2	5.26	11.5	1420	.211	1.66	A
110	5.93-8	287	1.78-5	1530				13.9	4.49	4.23	1445	.208	2.05	A
115	2.71-8	382	2.22-5	1494				5.02	3.81	1.86	1492	.201	2.32	C
120	1.48-8	477	2.58-5	1454	2.77	3.50	2.55	2.29	3.31	.990	1525	.197	2.49	C
125	9.03-9	571	2.92-5	1411	2.45	3.38	2.69	1.20	2.95	.576	1567	.192	2.64	C
130	5.95-9	665	3.22-5	1366	2.20	3.28	2.81	.692	2.63	.368	1582	.189	2.78	B
135	4.15-9	758	3.50-5	1326	1.99	3.16	2.93	.430	2.38	.250	1615	.186	2.90	B
140	3.02-9	850	3.73-5	1277	1.81	3.05	3.07	.283	2.16	.177	1642	.183	3.05	B
145	2.27-9	941	3.99-5	1228	1.65	2.92	3.24	.192	1.97	.129	1670	.180	3.23	B
150	1.76-9	1031	4.21-5	1180	1.52	2.82	3.40	.135	1.82	.0974	1715	.175	3.39	B
155	1.39-9	1120	4.45-5	1131	1.39	2.68	3.59	.0970	1.66	.0746	1738	.173	3.59	B
160	1.12-9	1207	4.64-5	1076	1.27	2.55	3.81	.0724	1.52	.0589	1765	.170	3.81	B

*$\mu = \frac{1458\times10^{-6} T^{3/2}}{T+110.4}$

†Assumes $\alpha = \frac{C\rho}{C_V} = 1.4$

†$T_o = T(1+\frac{\alpha-1}{2} m^2)$

A—Estimate Based on Aroesty's Data
B—Essentially Free-Molecule-Flow
C—Interpolated

here to a simple interpolation formula between Aroesty's data and free-molecular theory. The choice of formula is guided indirectly by the recent cylinder drag data of Maslach and Schaaf,[12] the very high Mach number sphere drag data of Masson, Morris and Bloxsom,[13] and general intuitive considerations of smoothness. For $Re_2 < 4$ the authors take

$$C_D(s, s_w, Re_2) = C_{D_{F.M.}}(s, s_w)\,[1 - Re_2(0.040 + 0.032\,s^{-4})]\,. \tag{4}$$

It is felt that this may apply fairly well over a range of values of T_w/T and with little dependence upon atmospheric composition, except for the influence of these quantities on $C_{D_{F.M.}}$.

The initial estimates of C_D, denoted $C_D^{(o)}$, and based on the ARDC 1959 Model Atmosphere, are tabulated in Table 1.

4. EXPERIMENTAL RESULTS

4.1 Rocket and Sphere Trajectory

The Aerobee 150 for this experiment was launched from the Eglin Gulf Test Range on Santa Rosa Island, Florida, on 7 December 1961, at 23:15:00.898 GMT (Fastax). Sphere ejection occurred 80.7 sec later at 285,000 ft and the sphere then coasted to a peak at 250.7 sec at 732,000 ft. Rocket vehicle peak was at 254.1 sec at 740,000 ft. The best trajectory for the rocket was obtained by the MPS-19 radar beacon. MATTS data provided accurate sphere time-space positioning which was used in the density calculations. This data checks with optical tracking as shown in Figure 8.

Sphere velocity determinations, shown in Figure 9, were done on a best-fit basis by using local values of acceleration due to gravity and horizontal velocity determined from values at the peak of the trajectory. The known horizontal velocity was 290 m/sec and was assumed constant during the period of interest. Any variation in horizontal velocity, resulting from some external force, would be registered by the accelerometers mounted within the sphere. The maximum measured acceleration during the period of interest was 0.1 G for about 1 sec or a velocity variation of 0.98 m/sec, which is an insignificant contribution to the previously determined velocities.

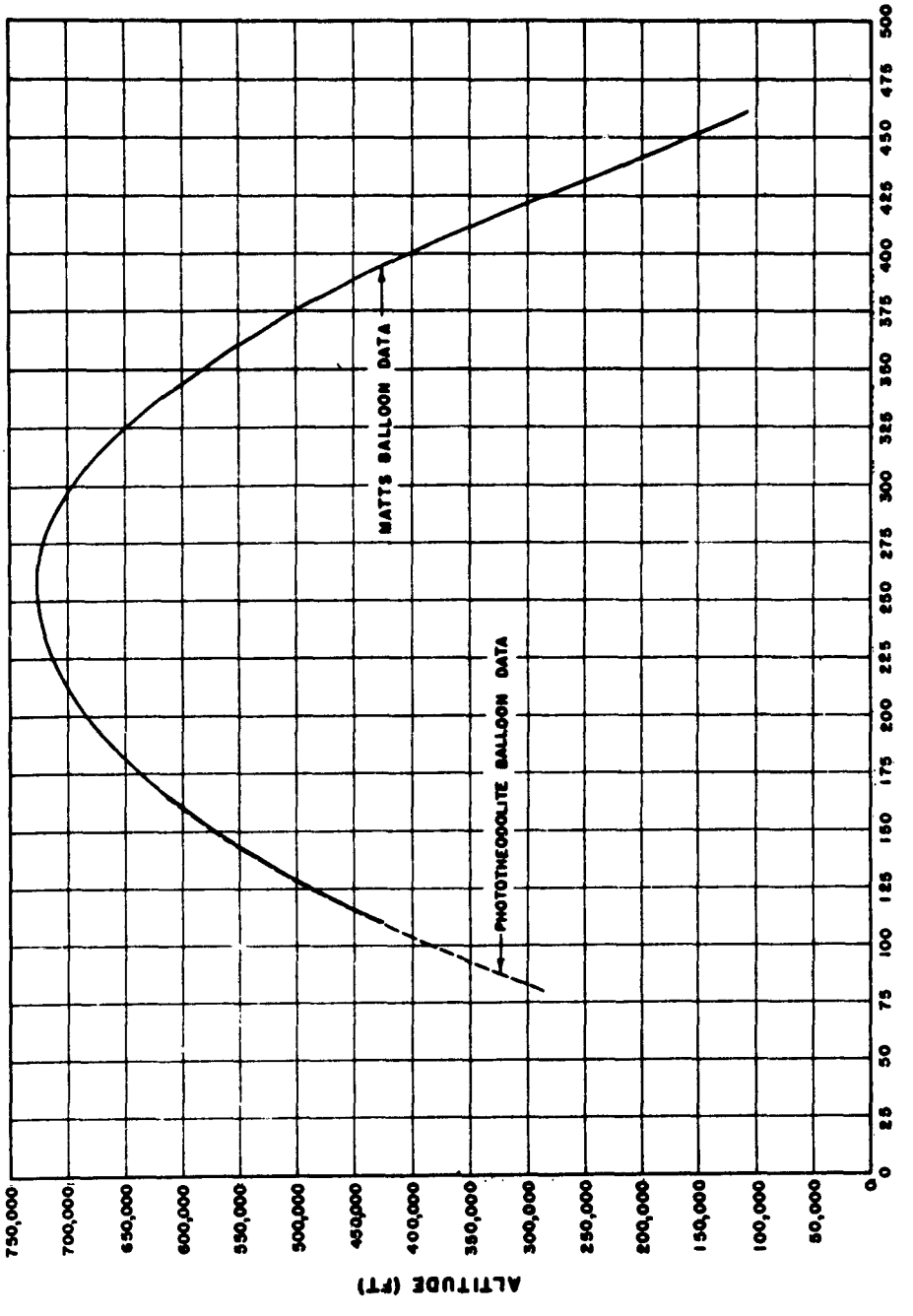

Figure 8. Comparison of Sphere Altitude vs Time (MATTS and Optical Data)

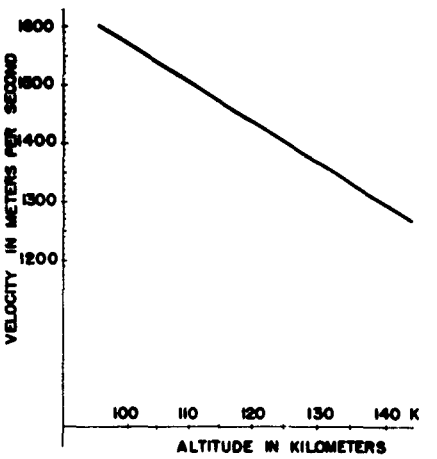

Figure 9. Sphere Velocity vs Time

4.2 Accelerometer Measurement

Figure 10 is the telemetry record for altitude 130 to 95 km, representing approximately 24 sec of the descent portion of this flight. These are the measured drag forces used in calculating the density profile for the experiment. The descent portion of the flight is selected because the sphere platform is more stable. The ascent portion of interest occurs immediately after ejection and time is required for structural rigidity and transitional accelerations to damp out. A wider range of more accurate measurements was possible on descent for this flight.

The telemetry record represents the measured accelerations along the X, Y, and Z axes of the sphere, shown as A_7, A_{10}, and A_{14} respectively. These axes are independent of the fixed earth axes used to determine altitude and velocity. The accelerometer measurements were telemetered in a nonlinear fashion with the greatest sensitivity at the low values of acceleration. This increases the dynamic range of the instrument, increasing the maximum altitude for the experiment. As can be seen from this telemetry record, the altitude span from 130 to 95 km is the extent of sensitivity. This is not an inherent limit but rather represents a particular design. At 95 km the readings are saturated and at 130 km the telemetered data uncertainty is large. The commutated telemetry signal at the top of Figure 10 includes, among other information, signals from three additional accelerometers. These accelerometers were included in this experiment as back-up instruments and were also aligned to measure accelerations along the X, Y, and Z axes. A less sensitive input voltage subcarrier channel was used for the commutated signal. All six units performed correctly and

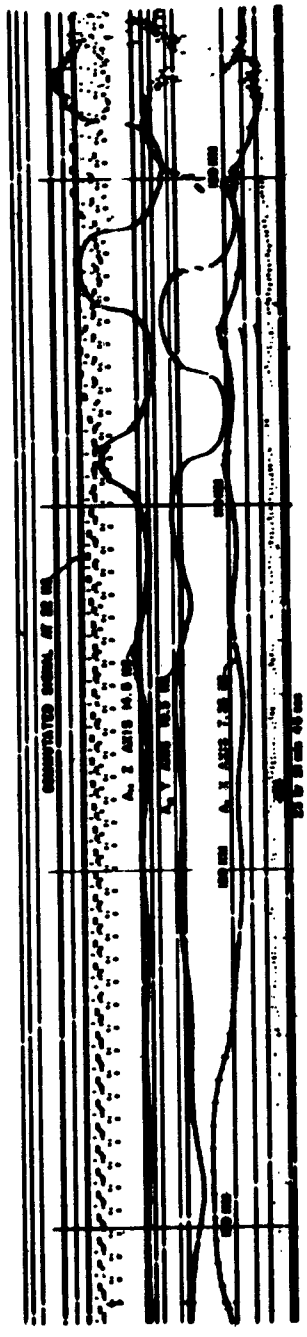

Figure 10. Telemetry Record for Altitude 130 to 95 km

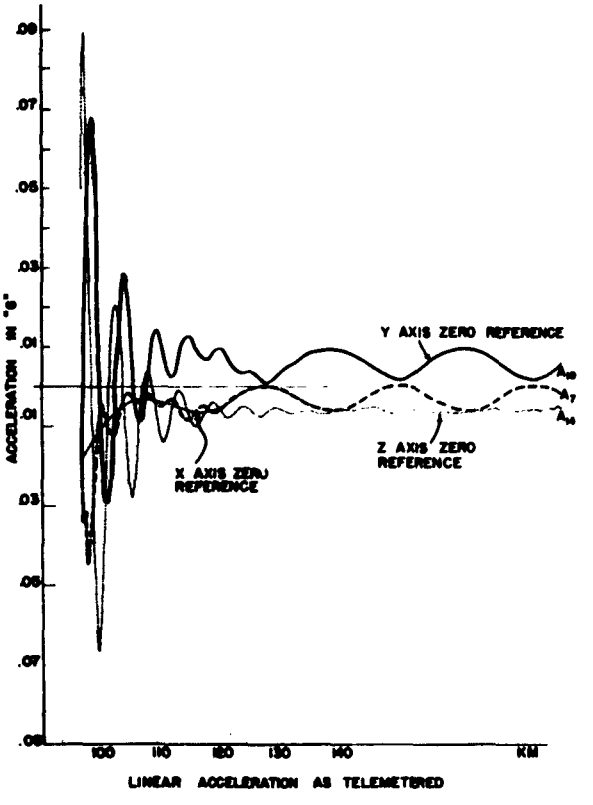

Figure 11. Uncorrected Values taken directly from Figure 10

a useful check was provided. This discounts any possibility of erroneous readings due to instrument malfunctions and certifies the curves of Figure 11 without explaining any discrepancies between measured and predicted values.

Figures 11 and 12 are plots of measured accelerations in G units vs altitude. Curves A_7, A_{10}, and A_{14} represent the X, Y, and Z axes respectively of the spinning sphere. Figure 11 presents the uncorrected values taken from the telemetry record. The only difference is that of plotting accelerations linearly instead of in a nonlinear function as displayed by the telemetry record. Figure 12 shows the corrected values of drag acceleration obtained from Figure 11. The question of major importance is "What accelerations need to be subtracted from the curves of Figure 11 to obtain true aerodynamic drag?" Figure 13 shows the vector sum or total drag acceleration from Figure 12.

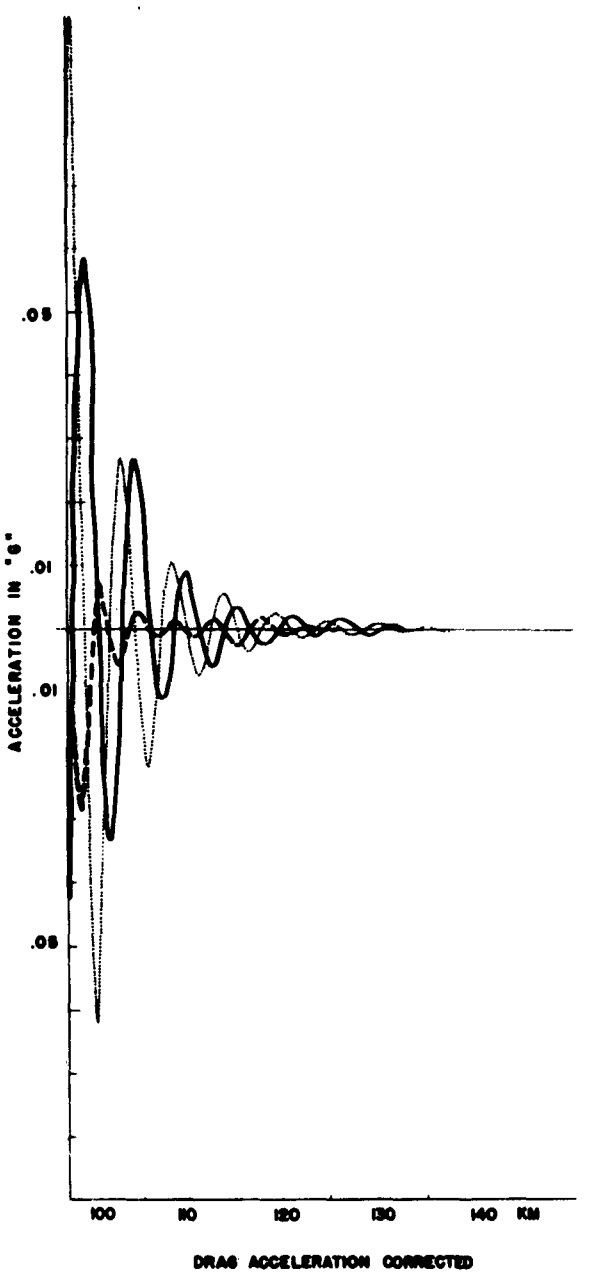

Figure 12. Corrected Values taken from Figure 11

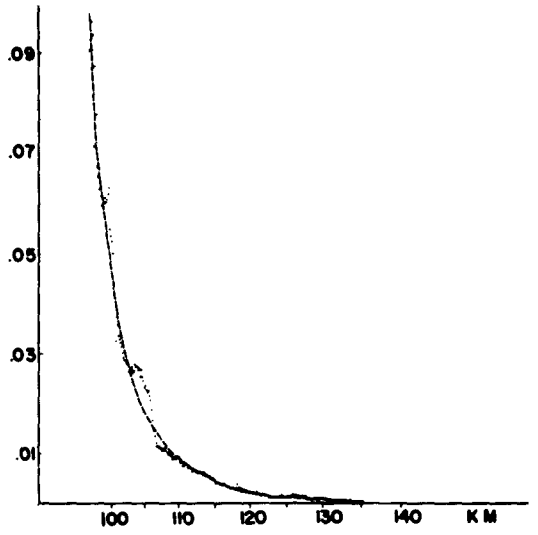

Figure 13. Sum Total Measured Drag Acceleration in G Units vs Altitude in Kilometers

4.3 System of Forces

For a first approximation the only forces experienced within a rigid spinning sphere in free fall are drag and centrifugal forces. The drag is related to velocity with respect to earth coordinates, and centrifugal acceleration arises from the spin of the sphere. It is not necessary to relate these independent sets of axes if the spin axis of the sphere remains arbitrarily constant with respect to its X, Y, Z system. In this case the centrifugal acceleration is determined by the normal distance to the spin axis R and the spin rate ω. If the accelerometer coincides with the spin axis, then this spurious acceleration will be zero. In practice $a_c = \omega^2 R$ is minimized. The drag occurs opposite the velocity vector of the sphere with respect to the ambient air. For high velocities in still air this is the direction of fall. Because the sphere is spinning about an arbitrary axis, the drag generally appears on all accelerometers as a sine function. When the sphere is entering the atmosphere the magnitude is always increasing. It is relatively easy to distinguish between the quantities $a = a_D + a_c$. This enables one to subtract the error a_c from Figure 11 and obtain true drag in Figure 12.

The system of forces acting is considerably more complicated than assumed above, resulting in accelerations that cannot always be disregarded. The sphere may be considered a solid, having a rotation. The effects that play an important part in this regard are: (1) the Poisson effect, (2) the Magnus effect, and (3) the

gyroscopic effect. Consider the case of a spin axis having a component normal to the direction of flow. For a right-hand rotation the Poisson effect results in a deviation to the right, the Magnus effect results in a deviation to the left, and the gyroscopic effect may result in a deviation in either direction. For small spin rates the gyroscopic effect will predominate. To calculate the magnitudes of these unwanted inputs to the accelerometer, one must know the orientation of the spin axis. It is possible to show that the sum effect for most of the downleg period of interest is small.

4.4 Drag Acceleration Results

To consider the practical circumstances, the sphere did not act as a rigid body. While the sphere instrument package was nearly 20 pounds, about two-thirds of this weight was concentrated in the instrument package located at the center and supported by two inflatable 6-inch struts fastened to the sphere at opposite points on the equator. This method of suspension is easier to package and, after ejection, should inflate easily with a minimum of disturbance to the structure. It appears that on a zero G trajectory (above 140 km) the system damps out sufficiently on only one axis—that which is most rigidly supported—along the strut. This is the Z axis of A_{14}.

Accelerometer A_{14} has a constant error corresponding to the centrifugal acceleration, a result of displacement from the spin axis. Neglecting other forces, a constant was subtracted from the values of Figure 11 to obtain Figure 12 values for this accelerometer. This may also be considered as subtracting the acceleration function experienced above 140 km where drag is known to be zero for the entire downleg portion. This function is the zero reference for drag purposes.

The zero reference or error to be subtracted from A_{10} is a periodic function. This apparently arises from harmonic motion of the strut in the cross-axis plane, a result of nonrigidity. The Y axis zero reference is subtracted from the curve of Figure 11 to obtain Figure 12. Since the aerodynamic drag has a frequency of about 1/3 cps and the zero reference has a much longer period, this can be done.

Accelerometer A_7 experiences the least amount of drag. The zero reference is not sufficient when extrapolated below 120 km, and a new zero reference for 95 to 120 km is indicated in Figure 11. This represents the values subtracted to obtain Figure 12. The basis for determining the zero level is the practical consideration that the drag which remains must have the same frequency component, 1/3 cps. This amounts to a graphical Fourier analysis, removing the undesirable frequency components and leaving the aerodynamic drag frequency.

Figure 13 represents the vector sum of the X, Y, and Z results of Figure 12, drag in G vs altitude in kilometers. Since C_D and sphere velocity have been determined it is now possible to obtain the density profile as determined by Eq. (1). Figure 14

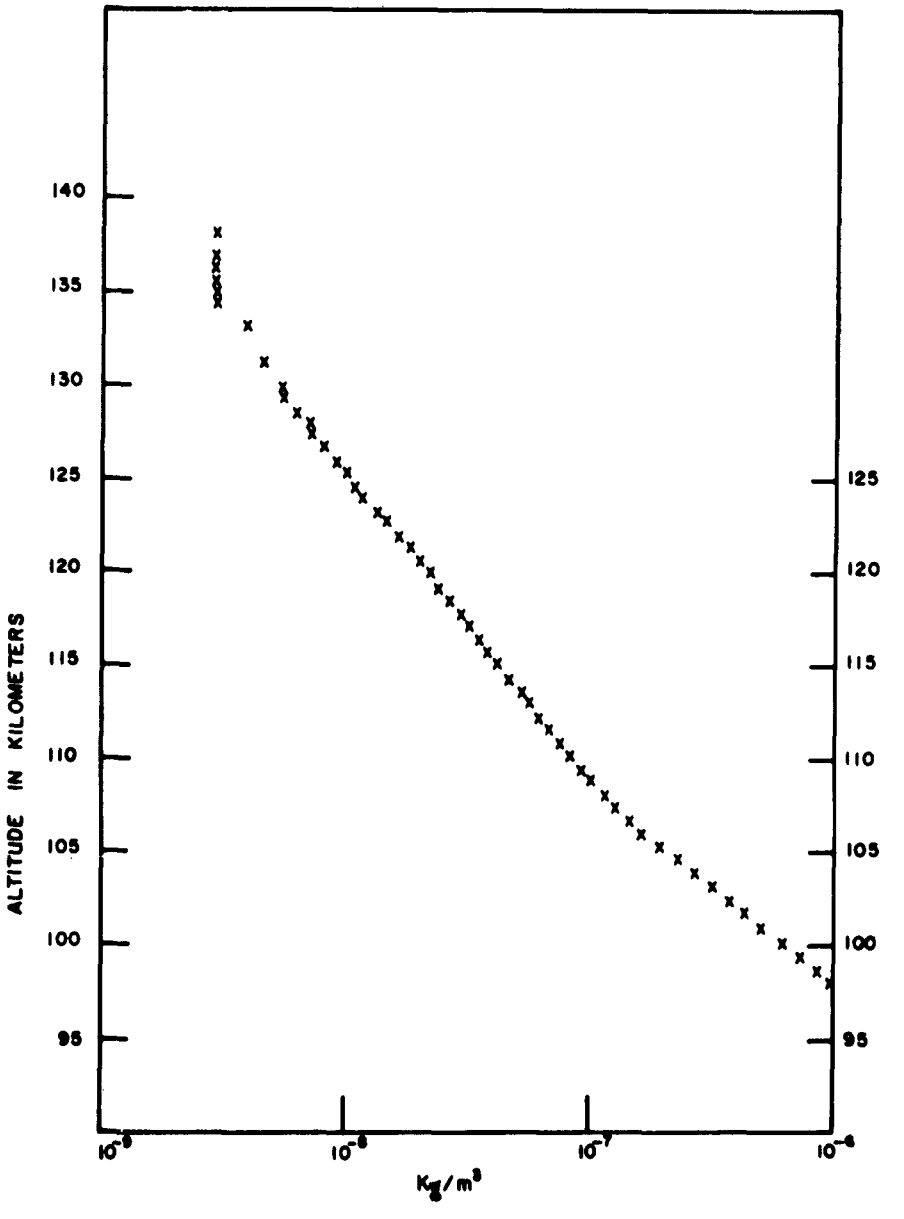

Figure 14. Calculated Density in Kilograms per Cubic Meters vs Altitude

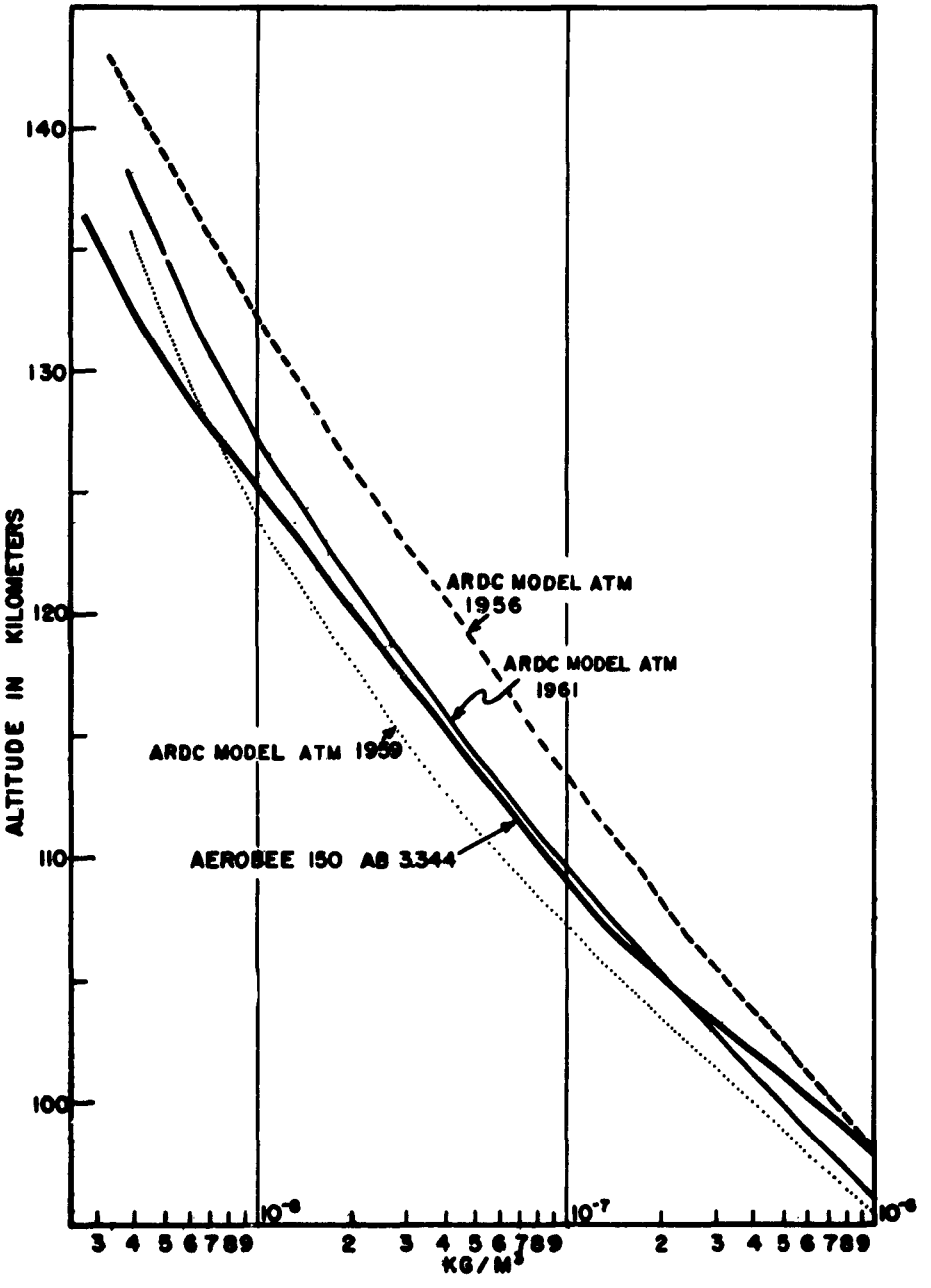

Figure 15. Compares Results with the ARDC Model Atmospheres, 1956, 1959, and 1961

shows the calculated density in kilograms per cubic meter vs altitude in kilometers, and Figure 15 compares results with the ARDC Model Atmospheres of 1956, 1959, and 1961.

5. ERRORS

The sources of error in the calculated density are: drag coefficient data, neglect of winds, calculation of the trajectory, and in measured values of A, m, and a_D. Drag acceleration a_D is the maximum source of error at present. The uncertainty in a_D arises not from the measuring instrument but from the interpretation of telemetered data to obtain true drag acceleration. This is particularly difficult in the case of a nonrigid sphere. Experimental uncertainties are given in Table 1.

5.1 Drag Coefficient Data

If the assumptions made in the earlier discussion regarding the reflection process in free-molecule flow are correct above 130 km (and the authors feel for many reasons that they are), the predicted C_D values in that regime should have no more than 2 or 3 percent probable error (due possibly to uncertainties in surface temperature). The estimated probable error of C_D values, where they actually overlap Aroesty's data (below 110 km), are approximately ± 2 percent. There are no firm guide lines for estimating error in the interpolation regime between free-molecule flow and Aroesty's data. Nonetheless the method of establishing the interpolation curves, their generally reasonable appearance, and the fact that they span only a relatively narrow gap between well-known anchor points give confidence that predictions made from these curves will also have probable errors of only a few percent. It would take a major distortion of any of these curves to move the probable error up or down by 5 percent of C_D.

5.2 Neglect of Wind

Motion of ambient air with respect to the sphere increases the effective drag velocity or the motion of the sphere with respect to the ambient atmosphere. Changes in wind speed of 100 m/sec have been observed from chemical releases within a height interval of 10 km. These winds are mainly horizontal and no vertical winds are thought to be significant in these altitude regions. Neglecting a vertical wind component causes a much larger error than neglecting a horizontal component of the same magnitude. However the nature of these winds is such that a variation with altitude usually exists and wind shears are often encountered.[14] As seen in Figure 13

the aerodynamic drag curve is not a smooth fit of any exponential curve. Certain errors are introduced in the ambient velocity especially at the lower altitudes of the flight regime. These errors are included in the total error estimates of Table 2.

TABLE 2.

Altitude (MATTS) km	C_D	Velocity (MATTS) m/sec	A_D Total Drag	ρ Density kg/m^3	% Error Pred. C_D	% Error Neglect of Winds	% Error in Traj.	% Error in Meas. of a_D	Net Prob. Error in Calculated Density
100	1.38	1591	47	5.94×10^{-7}	±2	2	>1	± 6	± 8%
105	1.66	1561	17.5	1.88×10^{-7}	±2	2	>1	±14	±17%
110	2.05	1530	8.5	8.40×10^{-8}	±2	2	>1	± 3	± 4%
115	2.32	1494	4.5	4.02×10^{-8}	5	1	>1	± 4	± 6%
120	2.49	1454	2.3	2.09×10^{-8}	5	1	>1	± 6	± 8%
125	2.64	1411	1.2	1.04×10^{-8}	5	1	>1	±18	±20%
130	2.78	1366	.6	5.05×10^{-9}	3	1	>1	±25	±30%
135	2.90	1326	.3	3.60×10^{-9}	3	1	>1	±49	±50%

5.3 Calculation of Trajectory

Errors in the calculation of the trajectory include errors in altitude that affect the position of the data on Figure 13 and errors because of velocity that enter into the equation. Position uncertainty of the sphere during descent through the period of interest was less than 100 m. Velocities at any point on the trajectory have two main sources of error: the horizontal velocity at peak and the error due to monitoring of external accelerations. The horizontal component was determined at peak to be 290 ± 20 m/sec. At the time of interest the vertical velocity is large and the contribution of the horizontal component to the vector sum is 6 percent or less. Thus the total error in velocity, as determined by the earth referenced system, is less than 1 percent.

5.4 Drag Acceleration

Errors in A and m can be made negligibly small with accurate weighing and good dimensions of the sphere. Errors associated with measurement and telemetry of acceleration are a function of magnitude due to the nonlinear method of deduction. The present limit on maximum altitude is determined by the telemetry input range.

At the appropriate range this error is less than 1 percent. As greater sensitivity is desired, then the methods of calibration degrade this figure. At the present state of the art these results could be extended in steps to altitudes of 160 km. Conversion of telemetered acceleration to drag values accounts for the unnecessarily large error (17 percent) at lower altitudes. This is due to the nonrigidity of the sphere. Consequently the spurious accelerations are larger and an uncertainty exists as to their exact function vs time. Determination of absolute error introduced in a_D requires knowledge of the rigidity of the sphere. This is most critical at higher values of a_D. At 115 km, 6 percent over-all uncertainty in the experiment gives a picture of the confidence in measurement. Total error estimates are given in Table 2.

6. ITERATIVE IMPROVEMENTS OF C_d ESTIMATES AFTER THE FLIGHT

From estimates of $C_D^{(o)}$ vs altitude, and with the measured velocity and drag force data, a first estimate of the density at the specific time and location of the sphere flight is derived. In the present case, the densities so derived—referred to as $\rho^{(1)}$—were substantially larger than those suggested in the ARDC Model Atmosphere, 1959. This fact, together with the evidence of the importance of solar-cycle and diurnal variations in atmospheric properties above 100 km,* makes it necessary to use the sphere drag data to the fullest extent possible to obtain self-consistency between the properties that were used to determine C_D and those deduced from it and the flight data.

The obvious iteration procedure is to use $\rho^{(1)}(h)$ and an assumed value of RT at the highest altitude for which density data were obtained (135 km) and then find $(RT)^{(1)}$ from the combined equations of hydrostatic equilibrium and of state. Thus

$$\rho^{(1)}(RT)^{(1)} = \rho_{135}^{(1)}\,(RT)_{135} - \int_{135}^{h} \rho\, g\, dt. \tag{5}$$

This procedure is arbitrary in its choice of RT at h = 135 km and in the decision to use only an arbitrary RT, multiplying it by a known $\rho_{135}^{(1)}$, rather than assuming an arbitrary ρ_{135}. Equation (5) has been integrated numerically, approximating the graph of $\rho^{(1)}\, g$ vs h by straigh-line segments for each Δh = 5 km, on a plot of log $[\rho^{(1)} g]$ vs h. This leads to the formula

$$-\int_{h_i}^{h_{i+1}} \rho\, g\, dt \approx \frac{(\rho g)_i - (\rho g)_{i+1}}{\ell n \dfrac{(\rho g)_i}{(\rho g)_{i+1}}}\,(h_{i+1} - h_i). \tag{6}$$

*See, for example, Harris and Priester.[11]

Several calculations were made to assess the sensitivity of derived estimates of RT to the assumed RT value at 135 km and to the scatter of the measured $\rho^{(1)}$ values around a smooth curve. In particular $(RT)_{135} = 2.23 \times 10^5$ km^2/sec^2 was tried from the ARDC 1959 Model and $(RT)_{135} = 1.48 \times 10^5$ km^2/sec^2 was tried from the NASA 1962 Model of Harris and Priester.[11] The latter value corresponds to Harris and Priester's solar activity parameter s = 100 (late 1961) and to a local flight time of 19:00 hours. Figure 16 shows the results of these integrations. As expected the curves converge and become essentially independent of $(RT)_{135}$ (and of $\rho^{(1)}$ for the uppermost two or three points, which were near the limit of experimental sensitivity) where $\rho^{(1)}$ (h) has become much greater than $\rho^{(1)}_{135}$. Thus the two curves start at $(RT)_{135}$ (ARDC) = 1.51 $(RT)_{135}$ (NASA), but are only 7 percent apart at h = 115 km and less than 1 percent apart at h = 100 km.

For the calculation of $C_D^{(1)}$ the authors chose to use the NASA $(RT)_{135}$, assuming this more recent prediction to be more applicable than the ARDC 1959 model. This resulted in a sizable increase in the Mach numbers and nearly doubled Re_2 at 100 km while slightly reducing it at 135. The net effect on C_D was a fairly uniform decrease, ranging from 4.8 to 8.9 percent. These values were then used to obtain second estimates of density, $\rho^{(2)}$, which were 5 to 9 percent higher than $\rho^{(1)}$. The hydrostatic equation was again integrated, using $\rho^{(2)}$, with the result that $(RT)^{(2)}$ differed at most by 2 percent from $(RT)^{(1)}$.

Finally a second iteration was performed to test convergence, and the resulting density estimates, $\rho^{(3)}$, differed by less than 1 percent from $\rho^{(2)}$. The final values cited as the experimental results of this flight are $\rho^{(3)}$ and $RT^{(2)}$, based on graphically smoothed values of $\rho^{(1)}$. Figure 17 shows this smoothed curve, together with the original point values and their probable errors.

Acknowledgments

The authors gratefully acknowledge the work of C.N. Stark who designed the ejection system for this experiment and who very capably described the system in GRD Research Notes No. 63 (see Reference 1). In addition, acknowledgment is made of the work of R.V. Matson and E.M. Carbary in carrying out these experiments, and of Capt. John H. Linebarger and the personnel of Eglin Gulf Test Range, Santa Rosa Island, Florida, who launched the rocket.

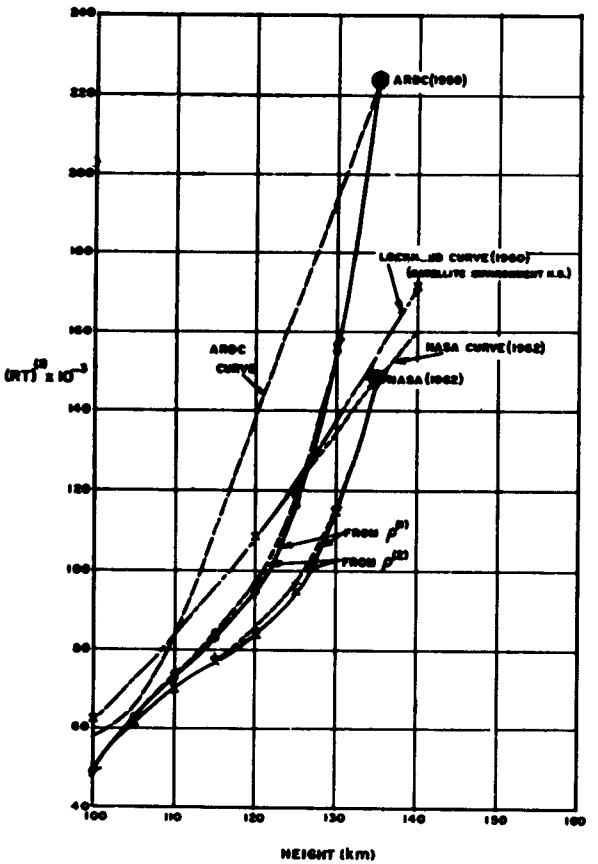

Figure 16. First Estimates of RT based on Sphere Drag Density Data $\rho^{(1)}$ and Assumed RT at h = 135 km[$\rho^{(1)}$ data smoothed]

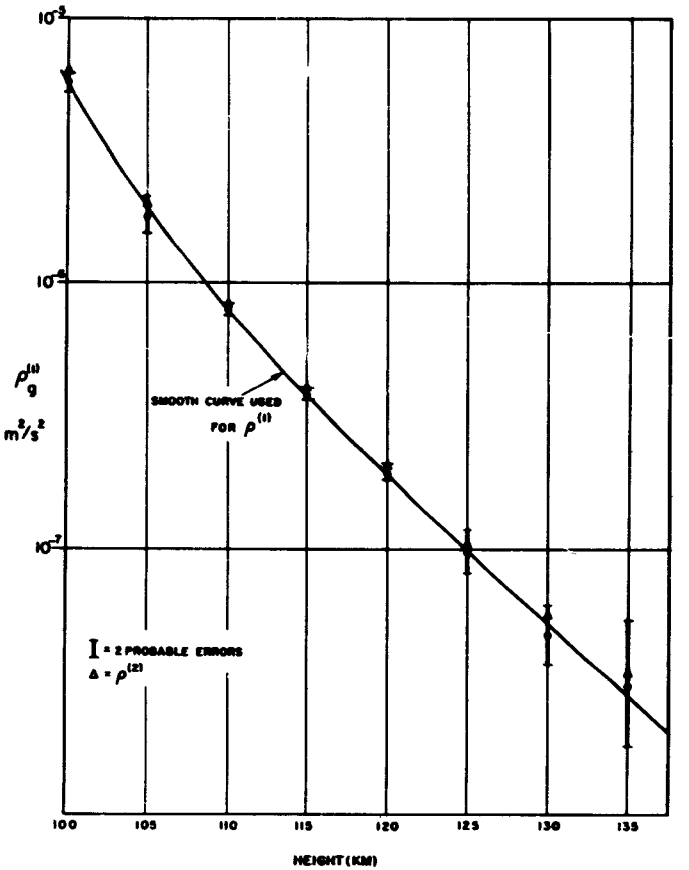

Figure 17. Final Values of Experimental Results

References

1. G.A. FAUCHER, R.W. PROCUNIER, and C.N. STARK, "Flight Information and Experimental Results of Inflatable Falling Sphere System for Measuring Upper Air Density" GRD Research Notes No. 63, AFCRL 695 (Aug 1961).
2. F.L. BARTMAN, et al. J. Atmos. and Terr. Physics, Spec. Suppl. 1 (1954).
3. F.L. BARTMAN, et al, "Upper Air Density and Temperature by the Falling Sphere Method," J. Appl. Physics (July 1956).
4. D. HOFFLEIT, "Dovap—A Method for Surveying High Altitude Trajectories," Scientific Monthly, 68, 172 (1949).
5. L.M. JONES and F.L. BARTMAN, "A Simplified Falling Sphere Method for Upper-Air Density" Eng. Res. Inst., Univ. of Michigan, Report 2215-10-T, (June 1956).
6. J.W. PETERSON, M/F Contract AF19(604)-1871 No. 2533-2-T, AFCRC-TN-56-870, "Analytical Study of the Falling-Sphere Experiment for Upper-Air Density Measurement" (1956).
7. J. AROESTY (1962), "Sphere Drag in a Low-Density Supersonic Flow," Univ. of Calif. IER Technical Report HE-150-192.*
8. H. ASHKENAS (1962), "Sphere Drag at Low Reynolds Numbers and Supersonic Speeds," JPL Cal Tech Research Summary 36-12, Section IX-A, page 93.*
9. A. SREEKANTH, "Drag Measurements of Circular Cylinders and Spheres in the Transition Region at a Mach Number of 2," UTIA Report 74, Univ. of Toronto (1961).
10. S.A. SCHAAF and P.L. CHAMBRÉ, "Flow of Rarefied Gases," Princeton Aeronautical Paperbacks, Princeton Univ. Press (1961).
11. I. HARRIS and W. PRIESTER, "Theoretical Models for the Solar-Cycle Variation of the Upper Atmosphere," NASA TN D-1444 (1962).
12. G.J. MASLACH and S.A. SCHAAF, " Cylinder Drag in the Transition from Continuum to Free Molecule Flow," Univ. of Calif. IER Technical Report HE-150-194 (1962).
13. D.J. MASSON, D.N. MORRIS, and D.E. BLOXSOM, "Measurements of Sphere Drag from Hypersonic Continuum to Free-Molecule Flow," pp 643-661 of Rarefied Gas Dynamics, Editor, L. Talbot, Academic Press, New York (1961).
14. K.S. CHAMPION and S.P. ZIMMERMAN (1962), "Winds and Turbulence at 200,000 to 400,000 feet from Chemical Releases" (to be published).
15. L.W. JONES and J.W. PETERSON, "Upper Air Densities and Temperatures Measured by the Falling Sphere Method" AFCRL-803, Contract AF19(604)-6185, U. of Michigan (Feb 1961).

*Papers to appear in Proceedings of the Third International Symposium on Rarefied Gas Dynamics, Paris, 1962. J. Laurmann, Editor, Academic Press, New York (in press).

AF Cambridge Research Laboratories, Bedford, Mass. Geophysics Research Directorate
UPPER-ATMOSPHERE DENSITY OBTAINED FROM FALLING SPHERE DRAG MEASUREMENTS, by G.A. Faucher, R.W. Procunier, and F.S. Sherman. December 1962. 27 pp incl. illus.
AFCRL-62-1136 Unclassified report

A density profile vs altitude from 95 to 130 km, obtained from drag measurements made directly from within a falling sphere, are presented. The main sensors are linear accelerometers aligned to measure X, Y, Z components of acceleration of the sphere from which total drag is obtained. The method consists of ejecting an inflatable sphere somewhere between 80 and 100 km on the ascent of an Aerobee 150 rocket flight. From ejection, the sphere continues to approximately 250 km altitude on a trajectory which is, except for drag, a free-fall trajectory. The prediction of sphere drag coefficients with their estimated probable errors are given in the altitude range from 90 to 160 km and was made
(over)

UNCLASSIFIED
1. Air Density-Measurements
2. Drag Acceleration—Measurements
3. Sphere—Drag Measurements

I. Faucher, G.A.
II. Procunier, R.W.
III. Sherman, F.S.

UNCLASSIFIED

AF Cambridge Research Laboratories, Bedford, Mass. Geophysics Research Directorate
UPPER-ATMOSPHERE DENSITY OBTAINED FROM FALLING SPHERE DRAG MEASUREMENTS, by G.A. Faucher, R.W. Procunier, and F.S. Sherman. December 1962. 27 pp incl. illus.
AFCRL-62-1136 Unclassified report

A density profile vs altitude from 95 to 130 km, obtained from drag measurements made directly from within a falling sphere, are presented. The main sensors are linear accelerometers aligned to measure X, Y, Z components of acceleration of the sphere from which total drag is obtained. The method consists of ejecting an inflatable sphere somewhere between 80 and 100 km on the ascent of an Aerobee 150 rocket flight. From ejection, the sphere continues to approximately 250 km altitude on a trajectory which is, except for drag, a free-fall trajectory. The prediction of sphere drag coefficients with their estimated probable errors are given in the altitude range from 90 to 160 km and was made
(over)

UNCLASSIFIED
1. Air Density—Measurements
2. Drag Acceleration—Measurements
3. Sphere—Drag Measurements

I. Faucher, G.A.
II. Procunier, R.W.
III. Sherman, F.S.

UNCLASSIFIED

AF Cambridge Research Laboratories, Bedford, Mass. Geophysics Research Directorate
UPPER-ATMOSPHERE DENSITY OBTAINED FROM FALLING SPHERE DRAG MEASUREMENTS, by G.A. Faucher, R.W. Procunier, and F.S. Sherman. December 1962. 27 pp incl. illus.
AFCRL-62-1136 Unclassified report

A density profile vs altitude from 95 to 130 km, obtained from drag measurements made directly from within a falling sphere, are presented. The main sensors are linear accelerometers aligned to measure X, Y, Z components of acceleration of the sphere from which total drag is obtained. The method consists of ejecting an inflatable sphere somewhere between 80 and 100 km on the ascent of an Aerobee 150 rocket flight. From ejection, the sphere continues to approximately 250 km altitude on a trajectory which is, except for drag, a free-fall trajectory. The prediction of sphere drag coefficients with their estimated probable errors are given in the altitude range from 90 to 160 km and was made
(over)

UNCLASSIFIED
1. Air Density-Measurements
2. Drag Acceleration Measurements
3. Sphere—Drag Measurements

I. Faucher, G.A.
II. Procunier, R.W.
III. Sherman, F.S.

UNCLASSIFIED

by Prof. Frederick S. Sherman of the University of California. The telemetry record showing the drag forces used in calculating the density profile in the altitude range 95 to 130 km is shown in Figure 10. The sources of error in the calculated density are analyzed and tabulated. The calculated density in kilograms per cubic meters vs altitude in kilometers is compared with the ARDC Model Atmospheres of 1956, 1959, and 1961.

UNCLASSIFIED

UNCLASSIFIED

by Prof. Frederick S. Sherman of the University of California. The telemetry record showing the drag forces used in calculating the density profile in the altitude range 95 to 130 km is shown in Figure 10. The sources of error in the calculated density are analyzed and tabulated. The calculated density in kilograms per cubic meters vs altitude in kilometers is compared with the ARDC Model Atmospheres of 1956, 1959, and 1961.

UNCLASSIFIED

UNCLASSIFIED

by Prof. Frederick S. Sherman of the University of California. The telemetry record showing the drag forces used in calculating the density profile in the altitude range 95 to 130 km is shown in Figure 10. The sources of error in the calculated density are analyzed and tabulated. The calculated density in kilograms per cubic meters vs altitude in kilometers is compared with the ARDC Model Atmospheres of 1956, 1959, and 1961.

UNCLASSIFIED

UNCLASSIFIED

by Prof. Frederick S. Sherman of the University of California. The telemetry record showing the drag forces used in calculating the density profile in the altitude range 95 to 130 km is shown in Figure 10. The sources of error in the calculated density are analyzed and tabulated. The calculated density in kilograms per cubic meters vs altitude in kilometers is compared with the ARDC Model Atmospheres of 1956, 1959, and 1961.

UNCLASSIFIED